


Determination of Optimal Separation Times for Dual-Pulse SWEEPS Laser-Assisted Irrigation in Different Endodontic Access Cavities

Matjaž Lukač,¹ Giovanni Olivi,² Mihnea Constantin,² Nejc Lukač,³ and Matija Jezeršek, PhD ^{3*}

¹Department of Complex Matter, Jozef Stefan Institute, Jamova cesta 39, 1000, Ljubljana, Slovenia

²Master Laser Dentistry, Catholic University of Sacred Heart-Rome, Largo Francesco Vito, 1, 00168, Rome, Italy

³Faculty of Mechanical Engineering, University of Ljubljana, Aškerčeva 6, 1000, Ljubljana, Slovenia

Background and Objectives: The purpose of this *ex vivo* study is to investigate whether it is possible to pre-determine and set the optimal separation times for the SWEEPS Er:YAG laser pulses pair during laser-assisted irrigation of endodontic root canals based on known lateral dimensions of the endodontic access cavities of different types of teeth.

Study Design/Materials and Methods: As the optimal SWEEPS laser pulse pair separation for enhanced shockwave generation depends on the life-cycle of a single-pulse bubble, measurements of the oscillation time T_B of the Er:YAG laser-generated bubble were made in 23 different endodontic access cavities of different types of teeth progressively widened in three different steps, into larger cavities, for a total of 69 cavities of different shapes and sizes. Different fiber-tip geometries (flat and radial), laser pulse energies (10 mJ and 20 mJ) and depth of fiber-tip insertion (2 mm and 4 mm) were also investigated. The obtained data were then analyzed using the reported relationship between the bubble oscillation time and the diameter of a cylindrically shaped cavity.

Results: A good fit to the relation analogue for ideal cylindrical cavities was found by taking the characteristic diameter of the access cavity to be represented by the cavity diameter either in the mesiodistal (D_{\min}) or buccolingual (D_{\max}) direction, or alternatively by the average of the two diameters (D_{ave}). The best fit was obtained for D_{\min} ($R^2 = 0.73$) followed in order by D_{ave} ($R^2 = 0.71$) and D_{\max} ($R^2 = 0.63$).

Conclusion: In spite of the endodontic cavities being non-cylindrical and of varied shape and size, the bubble oscillation time T_B and the corresponding optimal SWEEPS separation time can be well predicted using a single characteristic dimension of the access cavity. This finding enables a simple and practical method for determining optimal conditions for shock wave generation and enhanced photodynamic streaming in differently shaped and sized root canals, leading to improved treatment efficacy and safety of root canal irrigation. Lasers Surg. Med. © 2020 The Authors. Lasers in Surgery and Medicine published by Wiley Periodicals LLC

Key words: laser-activated irrigation; Er:YAG laser; root canal irrigation; dual-pulse

INTRODUCTION

The root canal preparation consists of mechanical instrumentation followed by chemical irrigation [1–3], which is the most critical stage for the elimination of the infected material from the root canal that includes removal of bacteria, vital, necrotic, and infected tissues [4–7]. Due to the highly complex anatomy of the root canal system [8], the standard method of hand syringe irrigation has been found unsatisfactory for cleaning and disinfecting the root canal wall from debris and bacteria [9,10]. For this reason, various other techniques such as negative pressure [11], sonic [12], and ultrasonic irrigation [13–15], and more recently laser-activated irrigation (LAI), have been introduced to enhance the irrigation action [16–23].

During LAI, short Erbium laser pulses (wavelength: 2.94 μm for Er:YAG and 2.78 μm for Er, Cr:YSGG) with durations in the range of 25 [24] to 200 μs [25] are delivered through a fiber tip (FT) into the irrigant-filled coronal access cavity. Due to the strong absorption of the Erbium wavelength in the irrigant, a vapor bubble is generated at the end of the submerged fiber tip [26]. The rapid expansion and collapse of the bubble results in secondary cavitation and fluid motion along the entire root canal system [18,27,28] leading to enhanced chemomechanical irrigation [19,29] when ethylenediaminetetraacetic acid and NaOCl solution are used as irrigants. This long-distance action of LAI represents

This is an open access article under the terms of the Creative Commons Attribution-NonCommercial License, which permits use, distribution and reproduction in any medium, provided the original work is properly cited and is not used for commercial purposes.

Conflict of Interest Disclosures: All authors have completed and submitted the ICMJE Form for Disclosure of Potential Conflicts of Interest and have disclosed the following: Two of the authors (Matjaž Lukač and Nejc Lukač) are affiliated also with Fotona, d.o.o.

*Correspondence to: Matija Jezeršek, Faculty of Mechanical Engineering, University of Ljubljana, Jamova cesta 39, 1000 Ljubljana, Slovenia. E-mail: matija.jezersek@fs.uni-lj.si

Accepted 7 November 2020

Published online 1 December 2020 in Wiley Online Library

(wileyonlinelibrary.com).

DOI 10.1002/lsm.23357

an important advantage in comparison to other irrigation techniques that require a different tip/needle to be inserted up to the apical area [12,30,31].

However, due to the friction on the cavity walls, the bubble oscillation is significantly slowed down, reducing the intensity of the bubble collapse within the root canal. Therefore, the shock waves that are usually emitted in the unconstrained environment following a bubble's collapse are decreased or not present at all [24,32].

To intensify the bubble collapse within the root canal, it has been proposed to use a dual-pulse modality, where the second laser pulse is applied just before the collapse of the first laser pulse's bubble [24,32,33]. The sudden expansion of the second bubble generated by the second laser pulse exerts additional pressure on the initial bubble, leading to its accelerated collapse, during which shock waves are emitted. Furthermore, shock waves are also emitted from the collapsing secondary cavitation bubbles that are formed throughout the entire length of the canal during laser-induced irrigation [24]. This dual-pulse LAI technique, named Shock Wave Enhanced Emission Photodynamic Streaming (SWEEPS), has been shown to result in significantly enhanced flushing action [34], and due to the increased pressure generation along the depth of the root canal, also results in enhanced penetration of irrigants into dentinal tubules [35,36], without increasing the risk of apical extrusion [37].

When the temporal separation (T_p) between the two SWEEPS laser pulses is fixed using the "X-SWEEPS" modality, the largest enhancement of shock waves and internal irrigant pressures occurs when T_p does not deviate substantially from the optimal separation time (T_{opt}), corresponding to the time when the second laser pulse of the X-SWEEPS pulse pair is delivered near the end of the collapse phase of the primary bubble generated by the first laser pulse ($T_{opt} \approx T_B$) [24,38].

A challenge involved in using X-SWEEPS in dental practice is posed by the fact that the bubble oscillation time T_B critically varies depending not only on laser parameters that can be controlled, but also on the endodontic access cavity dimensions that vary depending on the treated tooth, with T_B being longer for smaller cavity dimensions [24,38]. As an improved solution, a special AutoSWEEPS laser modality was developed [32,35,37] in which the temporal separation between the pair of laser pulses is continuously swept back and forth between $T_p = 200$ and $T_p = 650 \mu\text{s}$. This ensures that during each sweeping cycle there is always at least a $50 \mu\text{s}$ wide temporal separation range when the pulses are separated by $T_p \approx T_{opt}$, as required for optimal enhancement. The sweeping modality also ensures that the optimal conditions are approximately reached along the depth of the access cavity by matching the changing diameter conditions during the AutoSWEEPS cycle.

Under comparable conditions, the AutoSWEEPS modality has been reported to be about 50% more effective than the standard single-pulse SSP (super short pulse, $50 \mu\text{s}$ pulse duration) modality in generating pressures within the root canal and significantly better penetration

of irrigants into the dentinal tubules [35]. Also, as measured in laboratory conditions, the simulated debris removal rate of the AutoSWEEPS modality has been shown to be almost three times higher compared with that of the SSP modality [34]. Similarly, in a recent study, the efficacy of the removal of accumulated hard-tissue debris from the root canal system for AutoSWEEPS irrigation was compared with the SSP laser-assisted irrigation as well as with ultrasonically activated irrigation (UAI) using micro-computed tomography [39]. The AutoSWEEPS modality resulted in significantly improved debris removal in each portion of the root canals compared with SSP and UAI.

The aim of this study was to investigate whether it is possible to pre-determine and set the optimal SWEEPS pulse pair separation time T_{opt} based on the dimensions of the mesiodistal (lateral) side of the endodontic access cavity, to improve the LAI irrigation efficacy even further. Namely, the simulated debris removal rate of the X-SWEEPS modality has been observed to be higher by another factor of about three in comparison to that of the AutoSWEEPS modality in case of optimal pulse separation time selection [34]. In this order, bubble oscillation times were measured in differently sized access cavities, progressively widened in three different steps on extracted teeth for different fiber-tip geometries, laser pulse energies and depth of fiber-tip insertion. The obtained data was then analyzed using the reported dependence of the bubble oscillation time on the diameter of water-filled cylindrically shaped cavities [38]. A method for determining optimal separation times for typical cavity dimensions, fiber tip geometries and laser pulse energies is proposed.

MATERIALS AND METHODS

Experimental Setup

Twenty-three human teeth (eight upper and three lower molars, two upper and one lower premolars, two upper canines and three upper and four lower incisors) extracted for periodontal and/or orthodontic reasons were used in the study. Informed consent to the scientific use of the extracted teeth was signed by all the patients.

Endodontic access cavities were prepared in all extracted teeth using a round diamond bur. A specific shape of the access cavity was performed for each different tooth type. In order to simulate differently sized access cavities, as encountered in clinical practice. The access cavities were first minimally prepared, and then in two additional stages progressively widened into larger cavities. Thus, altogether, 3×23 differently sized and shaped access cavities were obtained and evaluated. The dimensions of the lateral side of the access cavities, prepared during each stage, were determined by measuring the mesiodistal (minor: D_{min}) and buccolingual (major: D_{max}) sides of the access cavity of each prepared anterior and posterior tooth (see Fig. 1a) using a microscope. The range of average diameters $D_{ave} = (D_{min} + D_{max})/2$ varied from 1.2

to 3.6 mm for the first preparation stage, from 1.86 to 4.32 mm for the second preparation stage, and from 2.13 to 6.18 mm for the last preparation stage. Note that repeated experiments on the same tooth do not influence the results as the LAI cleaning effects have a negligible effect on the size and shape of the access cavity where the bubble oscillation times were measured.

The prepared teeth were submerged in a water reservoir, and LAI was performed using an Er:YAG laser (LightWalker, Fotona d.o.o., Slovenia) equipped with a dental handpiece (H14, Fotona d.o.o., Slovenia) optically coupled with an interchangeable FT. The handpiece air/water spray was turned off during all experiments. The following FTs (manufactured by Fotona) were used in the study [35]:

- 1) Flat fiber tip; cylindrical flat-ended FT with 400 μm diameter (Flat Sweeps400, Fotona d.o.o., Slovenia).
- 2) Radial fiber tip; cylindrical radially-ended FT with 400 μm diameter (Radial Sweeps400, Fotona d.o.o., Slovenia).

The laser FT's end was positioned at two different depths in the access cavity, $h = 2$ or $h = 4$ mm (see Fig. 1b), using an XYZ micrometer positioning stage. The FT's position relative to the canal was monitored with a digital camera (Chameleon3, 1.3 MP; PointGrey, Richmond, Canada) with the optical resolution of 0.1 mm.

The bubble oscillation time was measured by "listening" to the sound of the explosive growth and collapse of the bubble using a microphone (Brüel & Kjær, Type 2669, Nærum, Denmark) positioned outside of the water reservoir. A typical signal is shown in Figure 2. As the X-SWEEPS pulse pair consists of two ultra short pulse (USP) laser pulses with duration of $t_p \approx 25 \mu\text{s}$, the

oscillation time of the primary bubble generated by the first pulse of the SWEEPS pulse pair was determined by measuring the oscillation time T_B of a single USP pulse. Single USP laser pulse energies of $E_L = 10$ mJ and 20 mJ were used.

Measurements were made for each endodontic access cavity geometry and laser activation condition (FT type, E_L and h).

Data Analysis

Recently [38], it was shown that for long liquid-filled cylindrical cavities (i.e., tubes) with diameter D_{cavity} , the bubble oscillation time T_B can be well described by a function:

$$T_B = T_{B,\text{inf}}(1 + K/D_{\text{cavity}}) \quad (1)$$

where K is the fitting parameter and $T_{B,\text{inf}}$ is the bubble oscillation time in an infinite reservoir ($D_{\text{cavity}} \approx \infty$) for a particular set of laser and FT parameters. The ratio $T_B/T_{B,\text{inf}}$ was found to be independent of the laser pulse energy E_L , with the best fit obtained for $K = 3.52$ mm where the statistical coefficient of determination $R^2 = 0.96$

Even though endodontic access cavities are relatively shallow and not cylindrically shaped, it was assumed that the access cavity bubble oscillation data can be approximated by a function similar to that in Equation (1):

$$T_B = T_0(1 + K_i/D_i) \quad (2)$$

where D_i represents one of the main lateral dimensions of the access cavity, D_{min} , D_{max} or D_{ave} , and K_{min} , K_{max} and K_{ave} are the corresponding fitting parameters. The time

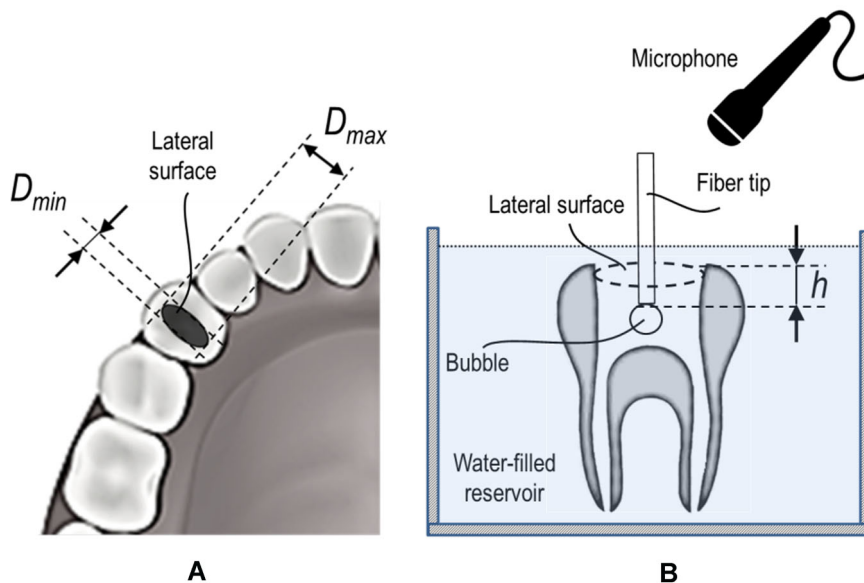


Fig. 1 (A) Mesiodistal (minor: D_{min}) and buccolingual (major: D_{max}) lateral sides of the endodontic access cavity, (B) experimental set-up.

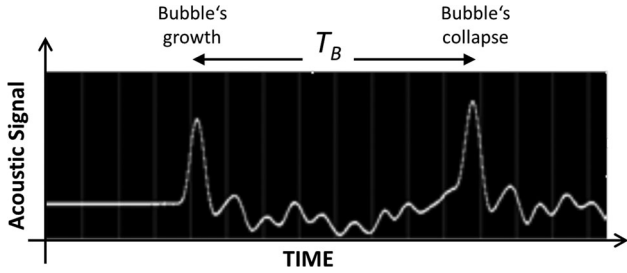


Fig. 2 The acoustic signal following the emission of a single Er:YAG laser pulse, displaying the initial rapid growth and final explosive collapse of the laser-generated bubble.

T_0 represents the bubble oscillation time for the infinitely wide endodontic access cavity ($D_i \approx \infty$).

RESULTS

Figure 3 shows the measured dependence of the bubble oscillation time (T_B) on the minor (mesiodistal) dimension (D_{min}) of the endodontic access cavity. The full lines represent fits to the function

$$T_B = T_0(1 + K_{min}/D_{min}) \quad (3)$$

with the same $K_{min} = 2.89$ for all fits, and the infinite cavity oscillation times T_0 as depicted in Table 1. Similar dependences were obtained also for D_{max} (with $K_{max} = 3.69$) and D_{ave} (with $K_{ave} = 3.35$).

Figure 4 depicts the obtained dependence of the ratio T_B/T_0 on D_{min} (Fig. 4a), D_{max} (Fig. 4b), and D_{ave} (Fig. 4c), with the best fit to Equation (2) obtained using $K_{min} = 2.89$, $K_{max} = 3.69$, and $K_{ave} = 3.35$.

Table 2 shows optimal separation times T_{opt} for mesiodistal cavity dimensions D_{min} in the range from 1 mm to 5 mm and for laser pulse energies of 10 mJ and 20 mJ. The average values are calculated using Equation (3) and $K = 2.89$ and the confidence interval ($\pm 50 \mu s$) was estimated from measurements presented in Figure 3.

DISCUSSION

The dimensions of endodontic access cavities vary significantly depending on the tooth type and size, dental tissue lost by decay and also on the endodontist's skill and preference when preparing it [7,40]. LAI bubble generation takes place in the coronal access cavity and accordingly its dimension variability effectively conditions the irrigant laser activation. Accordingly, when not using the AutoSWEEPS modality, the X-SWEEPS pulse temporal separation (T_p) would at least in principle have to be individually adjusted to the characteristics of each particular access cavity.

In a recent study of bubble dynamics in liquid-filled cylindrical tubes [38], it was shown that the bubble oscillation time (T_B) in a long tube can be predicted using a relatively simple relation between T_B and the tube's diameter D_{cavity} (see Equation 1). This enables predicting the optimal X-SWEEPS separation time in a cylindrically shaped cavity from the known diameter of the tube.

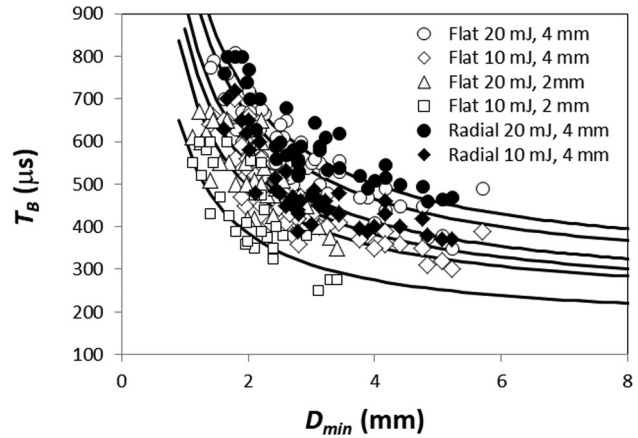


Fig. 3 Measured dependence of the bubble oscillation time T_B on the minor (mesiodistal) dimension of the endodontic access cavity for different FTs (Flat Sweeps400 and Radial Sweeps400), laser pulse energies E_L (in mJ) and insertion depths h (in mm). The lines represent the least square fits to Equation (3) using the same $K_{min} = 2.89$ for all fits, and T_0 as shown in Table 1. The bubble oscillation time measurement accuracy was $\pm 10 \mu s$.

In this *ex vivo* study, it was explored whether a similar relation can be found also for non-cylindrically shaped endodontic access cavities, with the access opening outline varying from ellipsoidal to trapezoidal shape. The results demonstrate that in spite of the varied shape and size of endodontic access cavities, the bubble oscillation time T_B can be well predicted using a single characteristic dimension D_i of the access cavity, represented by the cavity diameter either in the mesiodistal (D_{min}) or buccolingual (D_{max}) direction, or alternatively by the average of the two diameters (D_{ave}). The best fit to Equation (2) was obtained with D_{min} ($R^2 = 0.73$), followed in order by D_{ave} ($R^2 = 0.71$) and D_{max} ($R^2 = 0.63$). The observation that a single diameter can be used to describe the cavity size signifies that D_{min} and D_{max} are correlated to a certain degree, according to the conventional access cavity design rules [41,42]. We attribute the finding that D_{min} best defines the bubble oscillation time to the stronger

TABLE 1. Infinite Cavity Oscillation Times T_0 for Different FTs (Flat Sweeps400 and Radial Sweeps400), Laser Pulse Energies E_L (in mJ) and Insertion Depths h (in mm), as Obtained From Fitting the Experimental Data (Fig. 3) to Equation (3)

E_L (mJ)	h (mm)	Flat Sweeps400	Radial Sweeps400
		$T_0(\mu s)$	$T_0(\mu s)$
10	4	222 ± 10	239 ± 10
20	4	270 ± 10	290 ± 10
10	2	166 ± 10	$170 \pm 10^*$
20	2	214 ± 10	$220 \pm 10^*$

Exceptions are oscillation times marked with an * that were obtained from the measured ratios of bubble oscillation times for flat and radial tips inserted to $h=2$ mm in a simulated endodontic access cavity as used in [35].

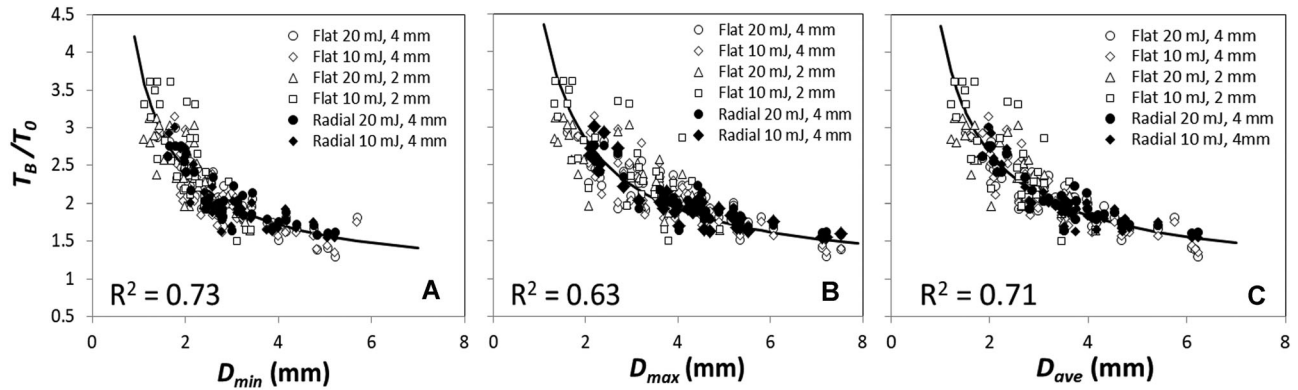


Fig. 4 Dependence of the ratio T_B/T_0 on D_{min} (A), D_{max} (B), and D_{ave} (C), with the best least squares fit (depicted by full lines) to Equation (2) obtained using $K_{min} = 2.89$ ($R^2 = 0.73$), $K_{max} = 3.69$ ($R^2 = 0.63$), and $K_{ave} = 3.35$ ($R^2 = 0.71$).

influence of the smaller dimension on the bubble dynamics.

The results of this study suggest a further potential improvement of the SWEEPS technique. Endodontic Er:YAG laser devices could be configured to enable the practitioner to define the optimal SWEEPS separation time by simply selecting the characteristic dimension D_i of the particular access cavity. As an example, Table 2 shows the optimal separation times T_{opt} for typical mesiodistal cavity dimensions D_{min} and typical laser pulse energies as calculated using Equation (3) and $K = 2.89$.

A limitation of this study is that the relation between access cavity dimension and bubble oscillation time presented with Equation (3) is validated only within a limited interval of cavity dimensions, from 1 to 6 mm, that however match the *in vivo* clinical conditions. Especially in a case of significantly smaller cavity dimension the bubble dynamics will deviate from the model assumption as it is described in [24]. A similar deviation is also expected in case the fiber tip is not positioned in the center of the cavity. As can be seen from the results (Fig. 3 and Table 1) the oscillation time also depends on the insertion depth of the fiber tip. This can be accurately controlled in the laboratory environment but more difficult to achieve under *in vivo* conditions where the fiber tip is manually positioned on a visual basis. Due to the above mentioned

limitations, the relation between T_B and D_i is only approximate, and the practitioner would potentially be only estimating the cavity size. However, an improved “Auto X-SWEEPS” modality could also be employed. This improved “Auto X-SWEEPS” modality would consist of the temporal separation between the pair of laser pulses being continuously swept back and forth between $T_{opt} - \Delta T_p$ and $T_{opt} + \Delta T_p$, where $\Delta T_p = 50 \mu s$ takes into account the observed spread of the actual bubble oscillation times around the predicted optimal separation times based on Equation (3) (See Fig. 4).

The possibility to significantly enhance the effective flushing action of SWEEPS [34], and to increase the pressure generation along the root canal [35,36], without increasing the risk of apical extrusion needs to be explored to assess the safety of “X-SWEEPS” modality. Studies in artificial models with apical constriction of ISO40 [37] and ISO45 [35] and lateral canal opening of ISO35 [35] indicate that the new SWEEPS method does not increase the risk of apical extrusion as compared with the single pulse LAI or standard syringe irrigation. Therefore, when all the parameters are correctly set, the possibility to maintain the irrigation efficacy while decreasing the energy to 15 mJ or 10 mJ [20], promises to offer a safe *in vivo* procedure also for larger apical opening.

TABLE 2. Optimal SWEEPS Pulse Separation Times (T_{opt}) for Typical Mesiodistal Cavity Dimension (D_{min}) at FT Insertion Depth of 4 mm

FT geometry	E_L (mJ)	Mesiodistal cavity dimension (D_{min})				
		1 mm	2 mm	3	4 mm	5 mm
Flat Sweeps400	10	$864 \pm 50 \mu s$	$543 \pm 50 \mu s$	$436 \pm 50 \mu s$	$382 \pm 50 \mu s$	$350 \pm 50 \mu s$
	20	$1050 \pm 50 \mu s$	$660 \pm 50 \mu s$	$530 \pm 50 \mu s$	$465 \pm 50 \mu s$	$426 \pm 50 \mu s$
Radial Sweeps400	10	$930 \pm 50 \mu s$	$584 \pm 50 \mu s$	$469 \pm 50 \mu s$	$412 \pm 50 \mu s$	$377 \pm 50 \mu s$
	20	$1128 \pm 50 \mu s$	$709 \pm 50 \mu s$	$569 \pm 50 \mu s$	$500 \pm 50 \mu s$	$458 \pm 50 \mu s$

CONCLUSIONS

In spite of the generically different dimensions and shapes of endodontic access cavities, the optimal pulse separation time (T_{opt}) between the two Er:YAG laser pulses of the X-SWEEPS modality, emitted at a specific pulse energy and with a specific fiber-tip diameter and shape, can be relatively well predetermined ($R^2 = 0.73$) and set for standardized volumes of different access cavities with longer separation times required for smaller cavity dimensions. This finding enables a relatively simple method for determining optimal conditions for shockwave generation and enhanced photodynamic streaming in differently shaped and sized root canals, leading to improved treatment efficacy and safety of root canal irrigation.

ACKNOWLEDGMENTS

This research was supported by the Ministry of Education, Science and Sport, Slovenia, under grants L2-1833, L3-7658, P2-0392, and Fotona d.o.o.

REFERENCES

- Stojicic S, Zivkovic S, Qian W, Zhang H, Haapasalo M. Tissue dissolution by sodium hypochlorite: Effect of concentration, temperature, agitation, and surfactant. *J Endod* 2010;36(9):1558–1562. <https://doi.org/10.1016/j.joen.2010.06.021>
- Zandi H, Rodrigues RC, Kristoffersen AK, et al. Antibacterial effectiveness of 2 root canal irrigants in root-filled teeth with infection: A randomized clinical trial. *J Endod* 2016;42(9):1307–1313. <https://doi.org/10.1016/j.joen.2016.06.006>
- Gazzaneo I, Vieira GCS, Pérez AR, et al. Root canal disinfection by single- and multiple-instrument systems: Effects of sodium hypochlorite volume, concentration, and retention time. *J Endod* 2019;45(6):736–741. <https://doi.org/10.1016/j.joen.2019.02.017>
- Hülsmann M, Peters OA, Dummer PMH. Mechanical preparation of root canals: Shaping goals, techniques and means. *Endod Top* 2005;10(1):30–76. <https://doi.org/10.1111/j.1601-1546.2005.00152.x>
- Peters OA. Current challenges and concepts in the preparation of root canal systems: A review. *Journal of Endodontics* Aug. 2004;30(8):559–567.
- Peters OA, Schönenberger K, Laib A. Effects of four Ni-Ti preparation techniques on root canal geometry assessed by micro computed tomography. *Int Endod J* 2001;34(3):221–230. <https://doi.org/10.1046/j.1365-2591.2001.00373.x>
- Castellucci A, West JD. Chapter 11 Access Cavity and Endodontic Anatomy. In: *Endodontics*. vol. 1. Firenze Il Tridente: Edizioni Martina, pp. 244–326.
- Vertucci FJ. Root canal anatomy of the human permanent teeth. *Oral Surg Oral Med Oral Pathol* 1984;58(5):589–599. [https://doi.org/10.1016/0030-4220\(84\)90085-9](https://doi.org/10.1016/0030-4220(84)90085-9)
- Walters MJ, Baumgartner JC, Marshall JG. Efficacy of irrigation with rotary instrumentation. *J Endod* 2002;28(12):837–839. <https://doi.org/10.1097/00004770-200212000-00011>
- Haapasalo M, Shen Y, Qian W, Gao Y. Irrigation in endodontics. *Dent Clin North Am* 2010;54(2):291–312. <https://doi.org/10.1016/j.cden.2009.12.001>
- Susin L, Yoon JC, Liu Y, et al. Canal and isthmus debridement efficacies of two irrigant agitation techniques in a closed system. *Int Endod J* 2010;43(12):1077–1090. <https://doi.org/10.1111/j.1365-2591.2010.01778.x>
- Bryce G, MacBeth N, Gulabivala K, Ng Y-L. The efficacy of supplementary sonic irrigation using the EndoActivator® system determined by removal of a collagen film from an ex vivo model. *Int Endod J* 2018;51(4):489–497. <https://doi.org/10.1111/iej.12870>
- Chan R, Versiani MA, Friedman S, et al. Efficacy of 3 supplementary irrigation protocols in the removal of hard tissue debris from the mesial root canal system of mandibular molars. *J Endod* 2019;45(7):923–929. <https://doi.org/10.1016/j.joen.2019.03.013>
- Lee S-J, Wu M-K, Wesselink PR. The effectiveness of syringe irrigation and ultrasonics to remove debris from simulated irregularities within prepared root canal walls. *Int Endod J* 2004;37(10):672–678. <https://doi.org/10.1111/j.1365-2591.2004.00848.x>
- Rödig T, Sedghi M, Konietschke F, Lange K, Ziebolz D, Hülsmann M. Efficacy of syringe irrigation, RinsEndo® and passive ultrasonic irrigation in removing debris from irregularities in root canals with different apical sizes. *Int Endod J* 2010;43(7):581–589. <https://doi.org/10.1111/j.1365-2591.2010.01721.x>
- De Moor RJG, Blanken J, Meire M, Verdaasdonk R. Laser induced explosive vapor and cavitation resulting in effective irrigation of the root canal. Part 2: Evaluation of the efficacy. *Lasers Surg Med* 2009;41(7):520–523. <https://doi.org/10.1002/lsm.20797>
- Kurzmann C, Meire MA, Lettner S, Farmakis ETR, Moritz A, De Moor RJG. The efficacy of ultrasonic and PIPS (photon-induced acoustic streaming) irrigation to remove artificially placed dentine debris plugs out of an artificial and natural root model. *Lasers Med Sci* 2020;35(3):719–728. <https://doi.org/10.1007/s10103-019-02912-3>
- de Groot SD, Verhaagen B, Versluis M, Wu M-K, Wesselink PR, van der Sluis LWM. Laser-activated irrigation within root canals: Cleaning efficacy and flow visualization. *Int Endod J* 2009;42(12):1077–1083. <https://doi.org/10.1111/j.1365-2591.2009.01634.x>
- DiVito E, Peters OA, Olivi G. Effectiveness of the erbium:YAG laser and new design radial and stripped tips in removing the smear layer after root canal instrumentation. *Lasers Med Sci* 2012;27(2):273–280. <https://doi.org/10.1007/s10103-010-0858-x>
- Golob BS, Olivi G, Vrabec M, El Feghali R, Parker S, Benedicenti S. Efficacy of photon-induced photoacoustic streaming in the reduction of *Enterococcus faecalis* within the root canal: Different settings and different sodium hypochlorite concentrations. *J Endod* 2017;43(10):1730–1735. <https://doi.org/10.1016/j.joen.2017.05.019>
- Arslan D, Kustarci A. Efficacy of photon-initiated photoacoustic streaming on apically extruded debris with different preparation systems in curved canals. *Int Endod J* 2018;51(Suppl 1):e65–e72. <https://doi.org/10.1111/iej.12816>
- Ozbay Y, Erdemir A. Effect of several laser systems on removal of smear layer with a variety of irrigation solutions. *Microsc Res Tech* 2018;81(10):1214–1222. <https://doi.org/10.1002/jemt.23122>
- De Meyer S, Meire MA, Coenye T, De Moor RJG. Effect of laser-activated irrigation on biofilms in artificial root canals. *Int Endod J* 2017;50(5):472–479. <https://doi.org/10.1111/iej.12643>
- Lukač N, Jezeršek M. Amplification of pressure waves in laser-assisted endodontics with synchronized delivery of Er:YAG laser pulses. *Lasers Med Sci* 2018;33(4):823–833. <https://doi.org/10.1007/s10103-017-2435-z>
- Yamazaki R, Goya C, Yu DG, Kimura Y, Koukichi Matsumoto K. Effects of erbium:chromium:YSGG laser irradiation on root canal walls: A scanning electron microscopic and thermographic study. *J Endod* 2001;27(1):9–12. <https://doi.org/10.1097/00004770-200101000-00003>
- Gregorčič P, Jezeršek M, Možina J. Optodynamic energy-conversion efficiency during an Er:YAG-laser-pulse delivery into a liquid through different fiber-tip geometries. *J Biomed Opt* 17(7):0750061. <https://doi.org/10.1117/1.JBO.17.7.075006>
- Lukač N, Zdravec J, Gregorčič P, Lukač M, Jezeršek M. Wavelength dependence of photon-induced photoacoustic streaming technique for root canal irrigation. *J Biomed Opt* 2016;21(7):75007. <https://doi.org/10.1117/1.JBO.21.7.075007>
- Matsumoto H, Yoshimine Y, Akamine A. Visualization of irrigant flow and cavitation induced by Er:YAG laser within a root canal model. *J Endod* 2011;37(6):839–843. <https://doi.org/10.1016/j.joen.2011.02.035>

29. Swimberghe RCD, De Clercq A, De Moor RJG, Meire MA. Efficacy of sonically, ultrasonically and laser-activated irrigation in removing a biofilm-mimicking hydrogel from an isthmus model. *Int Endod J* 2019;52(4):515–523. <https://doi.org/10.1111/iej.13024>
30. Lukač N, Gregorčič P, Jezeršek M. Optodynamic phenomena during laser-activated irrigation within root canals. *Int J Thermophys* 2016;37(7):66. <https://doi.org/10.1007/s10765-016-2071-z>
31. Koch JD, Jaramillo DE, DiVito E, Peters OA. Irrigant flow during photon-induced photoacoustic streaming (PIPS) using particle image velocimetry (PIV). *Clin Oral Invest* 2016;20(2):381–386. <https://doi.org/10.1007/s00784-015-1562-9>
32. Lukac N, Muc BT, Jezersek M, Lukac M. Photoacoustic endodontics using the novel SWEEPS Er:YAG laser modality. *J Laser Health Acad* 2017;1:1–7.
33. Gregorčič P, Lukač N, Možina J, Jezeršek M. Synchronized delivery of Er:YAG-laser pulses into water studied by a laser beam transmission probe for enhanced endodontic treatment. *Appl Phys A: Mater Sci Process* 2016;122(4):459. <https://doi.org/10.1007/s00339-016-9970-5>
34. Jezeršek M, Lukač N, Lukač M. Measurement of simulated debris removal rates in an artificial root canal to optimize laser-activated irrigation parameters. *Lasers Surg Med*. <https://doi.org/10.1002/lsm.23297>
35. Jezeršek M, Lukač N, Lukač M, Tenyi A, Olivi G, Fidler A. Measurement of pressures generated in root canal during Er:YAG laser-activated irrigation. *Photobiomodul Photomed Laser Surg* 2020;38(10):625–631. <https://doi.org/10.1089/photob.2019.4776>
36. Galler KM, Grubmüller V, Schlichting R, et al. Penetration depth of irrigants into root dentine after sonic, ultrasonic and photoacoustic activation. *Int Endod J* 2019;52(8):1210–1217. <https://doi.org/10.1111/iej.13108>
37. Jezeršek M, Jereb T, Lukač N, Tenyi A, Lukač M, Fidler A. Evaluation of apical extrusion during novel Er:YAG laser-activated irrigation modality. *Photobiomodul Photomed Laser Surg* 2019;37(9):544–550. <https://doi.org/10.1089/photob.2018.4608>
38. Lukač M, Lukač N, Jezeršek M. Characteristics of bubble oscillations during laser-activated irrigation of root canals and method of improvement. *Lasers Surg Med* 2020;52(9):907–915. <https://doi.org/10.1002/lsm.23226>
39. Yang Q, Liu MW, Zhu LX, Peng B. Micro-CT study on the removal of accumulated hard-tissue debris from the root canal system of mandibular molars when using a novel laser-activated irrigation approach. *Int Endod J* 2020;53(4):529–538. <https://doi.org/10.1111/iej.13250>
40. Alovisi M, Pasqualini D, Musso E, et al. Influence of contracted endodontic access on root canal geometry: An in vitro study. *J Endod* 2018;44(4):614–620. <https://doi.org/10.1016/j.joen.2017.11.010>
41. Krapež J, Fidler A. Location and dimensions of access cavity in permanent incisors, canines, and premolars. *J Conserv Dent* 2013;16(5):404–407. <https://doi.org/10.4103/0972-0707.117491>
42. Ingle JI, Bakland LK. *Endodontics*. 4th edition. Baltimore: Williams & Wilkins; 1994.